

Energetics of three interacting mass-imbalanced bodies in a three-dimensional spherical harmonic trap

A. D. Kerin¹ and A. M. Martin¹

¹*School of Physics, University of Melbourne, Parkville, VIC 3010, Australia*

(Dated: April 21, 2022)

We consider a system of three particles, either three identical bosons or two identical fermions plus an impurity, within an isotropic three-dimensional trap interacting via a contact interaction. Using two approaches, one using an infinite sum of basis states for the wavefunction and the other a closed form wavefunction, we calculate the allowable energy eigenstates of the system as a function of the interaction strength, including the strongly and weakly interacting limits. For the fermionic case this is done while maintaining generality regarding particle masses. We find that the two methods of calculating the spectrum are in excellent agreement and we find that both methods are unable to specify the energy of Efimov states and in fact the energies of Efimov states diverge in the same manner. We show that the numeric limitations of the summation approach correspond to the effective range boundary condition of the closed form approach to a high degree of accuracy.

I. INTRODUCTION

Ultracold quantum gases provide an ideal testbed for the investigation of many-body quantum systems. The foundation of such studies is the investigation of the properties of few-body systems [1–8]. Through solutions of the few-body problem it is possible to calculate the thermodynamics of many-body quantum gases [6, 9–18] and the quench dynamics of few-body systems [19–23]. Significant research has been undertaken [11, 24–26] into the study of the interacting three-body problem for both Bose and Fermi gases trapped in three-dimensional spherically symmetric harmonic traps. Such work has led to our understanding of Efimov states [25, 27–32] in Bose and mass-imbalanced Fermi systems.

In this work we consider two three-body systems: (i) a 2+1 fermion system, with mass imbalance between two substrate particles and an impurity particle and (ii) three identical bosons. In each case the particles interact via a contact interaction and are confined to a spherically symmetric harmonic trap. For the 2+1 Fermi system we derive, for general interaction strength and arbitrary mass imbalance between the substrate and impurity, the eigenspectrum for the system via a matrix approach [9]. For this system we also derive the system eigenstates in the unitary regime, where the s-wave contact interaction dominates. For comparison we revisit the solutions for the three boson system. For the 2+1 Fermi mass imbalanced system, as expected, we find Efimov like states using the matrix approach. This then leads us to revisit the effective range model for investigating Efimov states [25]. We find a connection between the numeric approach and the effective range approaches in determining that for a given matrix size there is a value of the effective range which produces, to a high degree of accuracy, the same energy spectrum.

II. OVERVIEW OF THE THREE-BODY PROBLEM

We consider a system of three interacting particles with arbitrary masses in a three dimensional spherically symmetric harmonic trap. The positions of the three particles are given \vec{r}_1 , \vec{r}_2 , and \vec{r}_3 with respective masses m_1 , m_2 , and m_3 . The Hamiltonian is given

$$\hat{H}_{3b} = \sum_{k=1}^3 -\frac{\hbar^2}{2m_k} \nabla_k^2 + \frac{m_k \omega^2 r_k^2}{2}, \quad (1)$$

and the inter-particle interactions are modelled as contact interactions enforced by the Bethe-Peierls boundary condition [33]. For convenience we define the following co-ordinate transformations,

$$\vec{C} = \frac{m_1 \vec{r}_1 + m_2 \vec{r}_2 + m_3 \vec{r}_3}{m_1 + m_2 + m_3}, \quad (2)$$

$$\vec{r} = \vec{r}_2 - \vec{r}_1, \quad (3)$$

$$\vec{\rho} = \frac{1}{\gamma} \left(\vec{r}_3 - \frac{m_1 \vec{r}_1 + m_2 \vec{r}_2}{m_1 + m_2} \right), \quad (4)$$

$$\gamma = \sqrt{\frac{m_1(m_1 + m_2 + m_3)}{(m_1 + m_2)(m_1 + m_3)}}.$$

We can then rewrite the Hamiltonian as

$$\hat{H}_{3b} = \hat{H}_{\text{COM}} + \hat{H}_{\text{rel}}, \quad (5)$$

$$\hat{H}_{\text{COM}} = -\frac{\hbar^2}{2M} \nabla_C^2 + \frac{M\omega^2 C^2}{2}, \quad (6)$$

$$\hat{H}_{\text{rel}} = -\frac{\hbar^2}{2\mu_{12}} \nabla_r^2 + \frac{\mu_{12}\omega^2 r^2}{2} - \frac{\hbar^2}{2\mu_{13}} \nabla_\rho^2 + \frac{\mu_{13}\omega^2 \rho^2}{2}. \quad (7)$$

where $\mu_{jk} = m_j m_k / (m_j + m_k)$ and $M = m_1 + m_2 + m_3$. \hat{H}_{COM} is the centre-of-mass (COM) part of the Hamiltonian, the solution to which is the simple harmonic oscillator (SHO) wavefunction, with mass M . \hat{H}_{rel} is the relative part of the Hamiltonian.

Throughout the rest of this paper we consider two specific cases. The first is two identical substrate fermions

interacting with a third impurity particle. For this case we set $m_1 = m_i$ and $m_2 = m_3 = m$, such that $\mu_{13} = \mu_{12} = \mu = m_i m / (m_i + m)$. The second case we consider is three identical interacting bosons. In this case $m_1 = m_2 = m_3 = m$ and $\mu_{13} = \mu_{12} = m/2$. For convenience we can in general define $\mu = m_i m / (m_i + m)$ where $m_i = m$ for the bosonic case. Finally we also define the COM harmonic length scale to be $a_{\text{COM}} = \sqrt{\hbar / (m_i + 2m)\omega}$, and the relative harmonic length scale to be $a_\mu = \sqrt{\hbar / \mu\omega}$, where again for bosons $m_i = m$.

For the fermionic case we investigate the effects of mass imbalance and so we define $\kappa = m/m_i$. The effects of changing κ are investigated in detail in Sections II A and II B. It should be noted that as the value of κ changes so too does a_μ . For this reason the $\kappa \rightarrow 0$ limit and $\kappa \rightarrow \infty$ limit must be defined as $m_i \rightarrow \infty$ (heavy impurity) and $m \rightarrow \infty$ (heavy substrate) respectively, as the masses tending towards zero would cause $\mu \rightarrow 0$ and thus $a_\mu \rightarrow \infty$. Due to the dependence of a_μ on κ we use a_m/a_s for $\kappa \leq 1$ and a_{m_i}/a_s for $\kappa \geq 1$ in Figs. 1, 2, and 3 where

$$\begin{aligned} a_\mu &= \sqrt{\frac{\hbar}{\mu\omega}} = \sqrt{1+\kappa} \sqrt{\frac{\hbar}{m\omega}} = \sqrt{1+\kappa} a_m, \\ &= \sqrt{\frac{\hbar}{\mu\omega}} = \sqrt{\frac{1+\kappa}{\kappa}} \sqrt{\frac{\hbar}{m_i\omega}} = \sqrt{\frac{1+\kappa}{\kappa}} a_{m_i}. \end{aligned} \quad (8)$$

In a non-interacting system Eqs. (6) and (7) can be solved with SHO wavefunctions. However, we impose the Bethe-Peierls boundary condition [33] to model a contact interaction,

$$\lim_{r_{ij} \rightarrow 0} \left[\frac{d(r_{ij} \Psi_{3b})}{dr_{ij}} \frac{1}{r_{ij} \Psi_{3b}} \right] = \frac{-1}{a_s}. \quad (9)$$

Here Ψ_{3b} is the total three-body wavefunction, $r_{ij} = |\vec{r}_i - \vec{r}_j|$, and a_s is the s-wave scattering length. The COM part of the wavefunction is independent of the boundary condition, and only the relative wavefunction is affected. Enforcing this boundary condition is equivalent to including a Fermi pseudo-potential term in the Hamiltonian [34].

If the wavefunction is symmetric under the interchange of particles j and k and satisfies the Bethe-Peierls boundary condition for r_{ij} then it satisfies the Bethe-Peierls boundary condition for r_{ik} . This relationship between particle interaction and particle interchange restricts us to the 2+1 fermion and three boson cases.

A. General interaction strength

By expressing the relative wavefunction as an expansion over basis states it is possible to obtain the allowable energy states for any value of a_s via a matrix eigenvalue problem [4, 9]. Due to the separability of the centre-of-mass and relative Hamiltonians the total three-body wavefunction may be written

$$\Psi_{3b}(\vec{C}, \vec{r}, \vec{\rho}) = \chi_{\text{COM}}(\vec{C}) \psi_{3\text{brel}}(\vec{r}, \vec{\rho}). \quad (10)$$

The centre of mass wavefunction, $\chi_{\text{COM}}(\vec{C})$, is a SHO wavefunction of lengthscale a_{COM} . The relative wavefunction, $\psi_{3\text{brel}}(\vec{r}, \vec{\rho})$, can be written

$$\begin{aligned} \psi_{3\text{brel}}(\vec{r}, \vec{\rho}) &= \\ &(1 + \hat{Q}) \sum_{n=0}^{\infty} C_n \psi_{2\text{brel}} \left(\nu_{nl}, \frac{r}{a_\mu} \right) R_{nl} \left(\frac{\rho}{a_\mu} \right) Y_{lm}(\hat{\rho}), \end{aligned} \quad (11)$$

where $\psi_{2\text{brel}}$ is the relative interacting two-body wavefunctions, first derived by Ref. [1], and ν_{nl} are the energy pseudo-quantum numbers. R_{nl} is the normalisation and radial part of the three dimensional SHO wavefunction and Y_{lm} is the spherical harmonic. \hat{Q} is the symmetrisation operator, it ensures the correct bosonic or fermionic symmetry of the wavefunction. For three identical bosons $\hat{Q} = \hat{P}_{13} + \hat{P}_{23}$, for two identical fermions and one distinct particle $\hat{Q} = -\hat{P}_{23}$, where \hat{P}_{jk} exchanges the location of particles j and k . The C_n terms are coefficients of expansion.

The energy of $\psi_{3\text{brel}}$ is given

$$E_{\text{rel}} = (2\nu_{nl} + 2n + l + 3)\hbar\omega, \quad (12)$$

where $\nu_{nl} + n$ is constant so that the energy of each term in Eq. (11) is the same.

The explicit form of the relative two-body wavefunction is [1]

$$\psi_{2\text{brel}}(\nu_{nl}, \tilde{r}) = N_{\nu_{nl}} e^{-\tilde{r}^2/2} \Gamma(-\nu_{nl}) U \left(-\nu_{nl}, \frac{3}{2}, \tilde{r}^2 \right), \quad (13)$$

$$N_{\nu_{nl}} = \sqrt{\frac{\nu_{nl} \Gamma(-\nu_{nl} - 1/2)}{2\pi^2 a_\mu^3 \Gamma(1 - \nu_{nl}) [\psi^{(0)}(-\nu_{nl} - 1/2) - \psi^{(0)}(-\nu_{nl})]}}$$

where U is Kummer's function, $\tilde{r} = r/a_\mu$ and $\psi^{(0)}$ is the digamma function of degree 0. The explicit form of R_{nl} is given

$$R_{nl}(\tilde{\rho}) = N_{nl}(\tilde{\rho})^l e^{-\tilde{\rho}^2/2} L_n^{l+\frac{1}{2}}(\tilde{\rho}^2), \quad (14)$$

$$N_{nl} = \sqrt{\frac{1}{4\pi a_\mu^6} \frac{2^{n+l+3} n!}{(2n+2l+1)!!}},$$

where $L_n^{l+\frac{1}{2}}$ is the associated Laguerre polynomial, and $\tilde{\rho} = \rho/a_\mu$. The exchange operators are given

$$\begin{aligned} \hat{P}_{23} f(\vec{C}, \vec{r}, \vec{\rho}) &= \\ &= f \left(\vec{C}, \frac{m\vec{r}}{m+m_i} + \gamma\vec{\rho}, \frac{(2m+m_i)m_i\vec{r}}{(m+m_i)^2\gamma} - \frac{m\vec{\rho}}{m+m_i} \right), \end{aligned} \quad (15)$$

where $m = m_2 = m_3$, $m_1 = m_i$ and

$$\begin{aligned} \hat{P}_{13} f(\vec{C}, \vec{r}, \vec{\rho}) &= \\ &= f \left(\vec{C}, \frac{m\vec{r}}{m+m_i} - \gamma\vec{\rho}, \frac{-(2m+m_i)m_i\vec{r}}{(m+m_i)^2\gamma} - \frac{m\vec{\rho}}{m+m_i} \right), \end{aligned} \quad (16)$$

where $m = m_1 = m_3$, $m_i = m_2$. In this paper \hat{P}_{13} is only applicable to the bosonic case where $m_1 = m_2 = m_3 = m_i = m$.

As per Ref. [9] the allowable values of the scattering length and expansion coefficients for a chosen energy (and thus chosen ν_{nl}) can be determined from the following matrix equation,

$$\frac{a_\mu}{a_s} \begin{bmatrix} C_0 \\ C_1 \\ \vdots \end{bmatrix} = \begin{bmatrix} X_{00l} & X_{01l} & X_{02l} & \dots \\ X_{10l} & X_{11l} & X_{12l} & \dots \\ \vdots & \vdots & \vdots & \ddots \end{bmatrix} \begin{bmatrix} C_0 \\ C_1 \\ \vdots \end{bmatrix}, \quad (17)$$

where

$$X_{n'n'l} = \frac{2\Gamma(-\nu_{n'l})}{\Gamma(-\nu_{n'l} - \frac{1}{2})} \delta_{n'n} - \eta \frac{(-1)^l}{\sqrt{\pi}} A_{n'n'l}, \quad (18)$$

and

$$A_{n'n'l} = \frac{a_\mu^3}{N_{\nu_{n'l}}} \int_0^\infty \tilde{\rho}^2 R_{n'l}(\tilde{\rho}) R_{n'l} \left(\frac{\kappa \tilde{\rho}}{1 + \kappa} \right) \times \psi_{2\text{brel}} \left(\nu_{n'l}, \sqrt{\frac{2\kappa + 1}{(1 + \kappa)^2} \tilde{\rho}^2} \right) d\tilde{\rho}, \quad (19)$$

and $\eta = -1$ or $\eta = 2$ for the fermionic and bosonic cases respectively. With Eqs. (17)–(19) the energy spectrum of the relative three-body wavefunction can be calculated for any desired value of κ .

Additionally in the $\kappa \rightarrow 0$ limit (the heavy-impurity limit) the matrix elements can be determined analytically:

$$A_{n'n,l} = \begin{cases} \frac{2}{n' - \nu} \sqrt{\frac{\Gamma(n + 3/2)\Gamma(n' + 3/2)}{\pi\Gamma(n + 1)\Gamma(n' + 1)}} & l = 0 \\ 0 & l > 0 \end{cases}. \quad (20)$$

However in the heavy substrate limit, $\kappa \rightarrow \infty$, Eq. (19) diverges due to $\psi_{2\text{brel}}(\nu, r)$ diverging as $r \rightarrow 0$.

The three-body energy spectrum is given in Figs. 1, 2, and 3. In Fig. 1 we present the fermionic energy spectrum for $\kappa = 1$ and $\kappa \rightarrow 0$ with $l = 0$. In Fig. 2 we present the bosonic energy spectrum for $l = 0$ and $l = 1$, recall $\kappa = 1$ for three identical bosons. In Fig. 3 we present the fermionic energy spectrum for $\kappa = 1$ and $\kappa = 13.75$ with $l = 1$. In all figures the horizontal black lines define the non-interacting energies and the vertical black lines are simply to indicate unitarity ($a_s \rightarrow \infty$).

B. Hyperspherical case

In Section II A we have derived the three-body relative wavefunction for general s-wave scattering length, a_s , and general mass ratio, κ , in the form of an infinite sum, Eq. (11). However, it is possible to derive a closed form expression for the wavefunction using hyperspherical coordinates [3, 35]. In the unitary and non-interacting cases all of the quantum numbers can be obtained exactly.

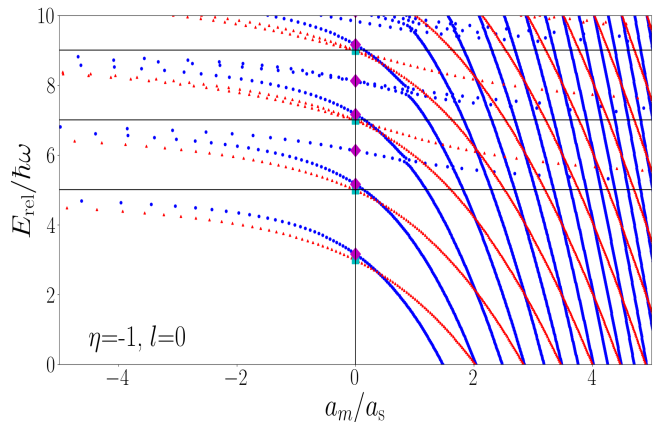


FIG. 1. Energy spectra of the fermionic three-body relative wavefunction, Eq. (11), for $l = 0$ calculated using Eq. (17) with a 50×50 matrix. Blue dots correspond to $\kappa = 1$ and red upright triangles to the $\kappa \rightarrow 0$ limit. The magenta diamonds are the unitary energies for $\kappa = 1$ and the cyan squares for $\kappa \rightarrow 0$, as per the calculations in Section II B. The solid horizontal black lines correspond to the non-interacting energies and the solid vertical black line is simply to indicate unitarity.

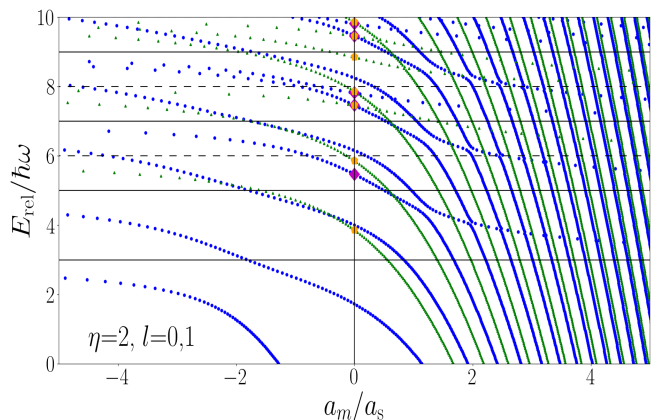


FIG. 2. Energy spectra of the bosonic three-body relative wavefunction, Eq. (11), calculated using Eq. (17) with a 50×50 matrix. Blue dots correspond to $l = 0$ and green inverted triangles to $l = 1$. The magenta diamonds are the unitary energies for $l = 0$ and the orange pentagons for $l = 1$, as per the calculations in Section II B. Some $l = 0$ unitary energies are unlabelled by a magenta diamond and these correspond to Efimov states as described in Section II C. The solid horizontal black lines correspond to the non-interacting energies of the $l = 0$ state and the dashed horizontal black lines to the $l = 1$ state. The solid vertical black line is simply to indicate unitarity.

We define the hyperradius, R , and the hyperangle, α ,

$$R = \sqrt{r^2 + \rho^2}, \quad \alpha = \arctan\left(\frac{r}{\rho}\right). \quad (21)$$

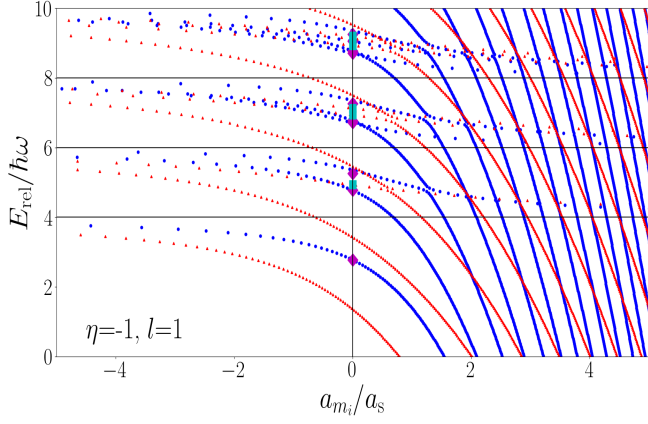


FIG. 3. Energy spectra of the fermionic three-body relative wavefunction, Eq. (11), for $l = 1$ calculated using Eq. (17) with a 50×50 matrix. Blue dots correspond to $\kappa = 1$ and red upright triangles to $\kappa = 13.75$. The magenta diamonds are the unitary energies for $\kappa = 1$ and the cyan squares for $\kappa = 13.75$, as per the calculations in Section II B. Some $\kappa = 13.75$ unitary energies are unlabelled by a cyan square and these correspond to Efimov states as described in Section II C. The solid horizontal black lines correspond to the non-interacting energies and the solid vertical black line is simply to indicate unitarity.

In turn the relative Hamiltonian is given

$$\hat{H}_{\text{rel}} = \frac{-\hbar^2}{2\mu} \left[\frac{\partial^2}{\partial R^2} + \frac{5}{R} \frac{\partial}{\partial R} + \frac{4}{R^2} \right. \\ \left. + \frac{1}{R^2 \sin^2(\alpha) \cos^2(\alpha)} \frac{\partial^2}{\partial \alpha^2} (\cos(\alpha) \sin(\alpha) \cdot) \right. \\ \left. - \frac{\hat{\Lambda}_\rho^2}{R^2 \cos^2(\alpha)} - \frac{\hat{\Lambda}_r^2}{R^2 \sin^2(\alpha)} \right] + \frac{\mu\omega^2 R^2}{2}, \quad (22)$$

where $\hat{\Lambda}_\rho^2$ and $\hat{\Lambda}_r^2$ are the angular part of the three-dimensional Laplace operators acting on the $\hat{\rho}$ and \hat{r} coordinate spaces respectively. The unnormalised solution is of the form

$$\psi_{\text{rel}} = \frac{a_\mu^2}{R^2} F_{qs_{nl}}(R) (1 + \hat{Q}) \frac{\varphi_{ls_{nl}}(\alpha)}{\sin(2\alpha)} Y_{lm}(\hat{\rho}). \quad (23)$$

Here q , l and s_{nl} are quantum numbers and give the energy

$$E_{\text{rel}} = (2q + l + s_{nl} + 1)\hbar\omega. \quad (24)$$

While q and l are non-negative integers the s_{nl} quantum number is more complicated. Following the work of Refs. [3, 10] several conditions can be placed on the wavefunc-

tion:

$$\varphi_{ls_{nl}}\left(\frac{\pi}{2}\right) = 0, \quad (25)$$

$$s^2 \varphi_{ls_{nl}}(\alpha) = -\varphi_{ls_{nl}}''(\alpha) + \frac{l(l+1)}{\cos^2(\alpha)} \varphi_{ls_{nl}}(\alpha), \quad (26)$$

$$E_{\text{rel}} F_{qs_{nl}}(R) = \frac{-\hbar^2}{2\mu} \left(F_{qs_{nl}}''(R) + \frac{F_{qs_{nl}}'(R)}{R} \right) \\ + \left(\frac{\hbar^2 s_{nl}^2}{2\mu R^2} + \frac{\mu\omega^2 R^2}{2} \right) F(R). \quad (27)$$

The first is enforced because a divergence at $\alpha = \pi/2$ is non-physical, the second and third come from requiring that Eq. (23) is an eigenfunction of Eq. (22). These conditions determine the functional form of the wavefunction. The hyperspherical solutions are given [10]

$$\varphi_{ls_{nl}}(\alpha) = \cos^{l+1}(\alpha) {}_2F_1 \left(\frac{l+1-s_{nl}}{2}, \frac{l+1+s_{nl}}{2}; l + \frac{3}{2}; \cos^2(\alpha) \right), \quad (28)$$

$$F(R) = \left(\frac{R}{a_\mu} \right)^{s_{nl}} e^{-R^2/2a_\mu^2} L_q^{s_{nl}} \left(\frac{R^2}{a_\mu^2} \right), \quad (29)$$

where ${}_2F_1$ is the Gaussian hypergeometric function. This solution for $F(R)$ is valid for $s_{nl}^2 \geq 0$. For $s_{nl}^2 < 0$ there is a different solution, see Section II C. Note that some values of s_{nl} and l are forbidden and are not predicted by the method of Section II A; $l = 0, s = 2$ for fermions and, $l = 1, s = 3$ and $l = 0, s = 4$ for bosons are forbidden because the wavefunctions are 0 [35].

The interactions are enforced by the Bethe-Peierls boundary condition, Eq. (9), and this allows for the values of s_{nl} to be calculated, but only in the non-interacting and unitary regimes. Note in Eq. (27) s_{nl}^2 appears not s_{nl} . Hence there is a degree of arbitrariness in s_{nl} , convention is to choose $s_{nl} \in [0, \infty)$ for $s_{nl}^2 \geq 0$ and $s_{nl} \in i \cdot [0, \infty)$ for $s_{nl}^2 < 0$. The $s_{nl}^2 < 0$ case will be considered in more detail in Section II C.

In the non-interacting case Eq. (9) implies $\varphi_{ls_{nl}}(0) = 0$, and so the values of s_{nl} are given

$$\text{NI fermions } s_{nl} = \begin{cases} 2n + 4 & l = 0 \\ 2n + l + 2 & l > 0 \end{cases}, \quad (30)$$

$$\text{NI bosons } s_{nl} = \begin{cases} 2 & l = 0 \\ 2n + 6 & l = 0 \\ 2n + l + 4 & l = 1 \\ 2n + l + 2 & l > 1 \end{cases}, \quad (31)$$

where $n \in \mathbb{Z}_{\geq 0}$.

In the unitary limit s_{nl} will solve the following transcendental equation

$$0 = \frac{d\varphi_{ls_{nl}}}{d\alpha} \Big|_{\alpha=0} + \eta(-1)^l \frac{(1+\kappa)^2}{\kappa\sqrt{1+2\kappa}} \varphi_{ls_{nl}} \left(\arctan \left(\frac{\sqrt{1+2\kappa}}{\kappa} \right) \right). \quad (32)$$

		3 bosons	2+1 fermions $\kappa = 1$	$\kappa = 13.75$
l	n	s_{nl}		
0	0	$i \cdot 1.006\dots$	2.166...	3.538...
	1	4.465...	5.127...	4.802...
	2	6.818...	7.114...	6.715...
	3	9.324...	8.832...	10.912...
1	0	2.863...	1.77...	$i \cdot 0.165\dots$
	1	6.462...	4.358...	3.940...
	2	7.852...	5.716...	6.132...
	3	9.822...	8.053...	8.211...
2	0	2.823...	3.104...	3.853...
	1	5.508...	4.795...	4.965...
	2	6.449...	7.238...	6.707...
	3	9.272...	8.837...	8.782...
3	0	4.090...	3.959...	3.383...
	1	5.771...	6.127...	6.062...
	2	8.406...	7.816...	8.196...
	3	9.607...	10.172...	10.200...

TABLE I. Three-body wavefunction eigenvalues, s_{nl} , at unitarity for the bosonic case and the fermionic case with $\kappa = 1$ and $\kappa = 13.75$, to three decimal places.

See Table I for solutions to Eq. (32).

In the $\kappa \rightarrow 0$ limit, with $\eta = -1$ (fermions), Eq. (32) reduces to

$$0 = \left. \frac{d\varphi_{ls_{nl}}}{d\alpha} \right|_{\alpha=0} - \delta_{l,0}, \quad (33)$$

in turn this implies, for $\kappa \rightarrow 0$,

$$s_{nl} = \begin{cases} 4n + 2 & l = 0 \\ 2n + l + 1 & l > 0 \end{cases}, \quad (34)$$

where $n \in \mathbb{Z}_{\geq 0}$. Note $l = 0, s = 2$ is normally forbidden and because $s \rightarrow 2$ as $\kappa \rightarrow 0$ this is never violated for finite mass imbalance. In the $\kappa \rightarrow \infty$ limit the right-hand term in Eq. (32) diverges unless s_{nl} takes specific values that cause the $\varphi_{ls_{nl}}$ part of the term to be 0. This implies, for $\kappa \rightarrow \infty$

$$s_{nl} = \begin{cases} 2n + 4 & l = 0 \\ 2n + l + 2 & l > 0 \end{cases}, \quad (35)$$

where $n \in \mathbb{Z}_{\geq 0}$.

The energies at unitarity are plotted in Figs. 1, 2 and 3. In Fig. 1 the purple diamonds indicate unitary energies for the $\kappa = 1$ case and the cyan squares for the $\kappa \rightarrow 0$ case. In Fig. 2 the purple diamonds indicate the unitary energies for $l = 0$ and the orange pentagons for $l = 1$. In Fig. 3 the purple diamonds indicate unitary energies for the $l = \kappa = 1$ case and the cyan squares for $l = 1$ and $\kappa = 13.75$.

The energies calculated using the general method of Section II A are in excellent agreement with the hyperspherical approach of this section. However, as noted

in the captions of Figs. 2 and 3, some states are not marked at unitarity with an energy from a hyperspherical calculation. These states are Efimov states and they correspond to the case where s_{nl} is imaginary. In this case Eq. (29) is not the correct wavefunction and so $E_{\text{rel}} = (2q + s_{nl} + 1)\hbar\omega$ is not applicable.

C. Efimov states

The previous two sections have investigated the agreement between two different methods of calculating the unitary energy spectrum of trapped three-body systems with mass imbalance. We find that the two methods are in excellent agreement, however, as noted in Figs. 2 and 3, there are some unitary energies predicted by the method of Section II A that are not predicted by the method of Section II B. These unmarked states, associated with imaginary values of s_{nl} , are Efimov states, e.g. s_{00} for bosons and s_{01} for $\kappa = 13.75$ fermions.

Eq. (27) is the Schrödinger equation for a particle moving in a two dimensions with two potential terms, a harmonic potential and a term proportional to s_{nl}^2/R^2 . If s_{nl} is purely imaginary then this potential is *attractive* at short distances rather than repulsive. This necessitates a different class of solution compared to the case where s_{nl} is purely real and these solutions are Efimov states. Physically speaking the Efimov effect is short-range interparticle interactions giving rise to an effective attractive long-range interaction due to a third particle mediating the effective interaction between the other two.

These states were first studied in Ref. [28] in the free context and Ref. [25] in a trapped context. Efimov states were first observed in an ultracold gas in Ref. [36].

For imaginary s_{nl} the hyperradial solution is given [3]

$$F(R) = \frac{a_\mu}{R} W_{\frac{E_{\text{rel}}}{2\hbar\omega}, \frac{s_{nl}}{2}} \left(\frac{R^2}{a_\mu^2} \right), \quad (36)$$

where $W_{a,b}(x)$ is the Whittaker function. In the universal ($s_{nl}^2 > 0$) case Eqs. (27) and (29) imply $E_{\text{rel}} = (2q + s_{nl} + 1)\hbar\omega$. However, in the Efimov case the relative energy is left a free parameter. Using the method of Section II A the energies of the Efimov states do not converge to a constant value as the matrix size is increased, whereas the universal states do converge. This non-convergence of the Efimov states is shown in Fig. 4, where the change in energy, $\Delta E = (E - E_{N=10})/E_{N=10}$ is plotted as a function of the matrix size (N) in Eq. (17). Figs. 4(a) and 4(b) plot ΔE for bosons and fermions respectively. From these plots it is clear that as N is increased the energy for the universal states ($s_{nl}^2 > 0$) states remains constant, whereas the Efimov state energies diverge. This divergence arises from the fact that the Hamiltonian and Bethe-Peierls boundary condition do not contain enough information to uniquely specify the energies of the Efimov states. We find that the Efimov energies diverge logarithmically. As such an addi-

tional boundary condition is needed to fix the Efimov energies.

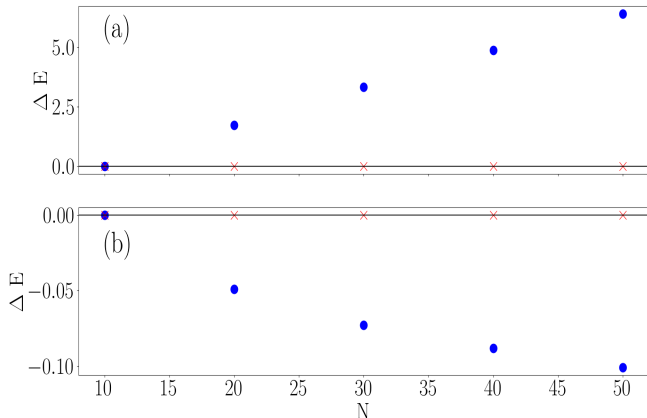


FIG. 4. The relative change the energies of the $q = 0$ Efimov (blue circles) and lowest energy universal (red crosses) states calculated as per Section II A with increasing matrix size in Eq. (17). N is the dimension of the matrix, i.e. matrix is $N \times N$, and $\Delta E = (E - E_{N=10})/E_{N=10}$ is the proportional deviation away from the $N = 10$ energy (universal or Efimov as appropriate). Panel (a) is the bosonic $l = 0$ case ($E_{N=10} = -0.563\hbar\omega$) and the panel (b) is the fermionic $l = 1$, $\kappa = 13.75$ case ($E_{N=10} = 1.507\hbar\omega$). The horizontal black line defines $\Delta E = 0$.

The Efimov hyperradial function, Eq. (36), oscillates increasingly rapidly as $R/a_\mu \rightarrow 0$ (but remains bounded). To find the Efimov states we require the phase of the oscillation to be fixed, and impose the boundary condition

$$F(R) \underset{R \rightarrow 0}{=} A \sin \left[|s_{0l}| \ln \left(\frac{R}{a_\mu} \right) - |s_{0l}| \ln \left(\frac{R_t}{a_\mu} \right) \right], \quad (37)$$

where A is a constant and $R_t > 0$ is the three-body parameter. The short range behaviour of the Efimov hyperradial wavefunction is given

$$\begin{aligned} \frac{a_\mu}{R} W \frac{E}{2\hbar\omega}, s_{0l} \left(\frac{R^2}{a_\mu^2} \right) \underset{R \rightarrow 0}{=} & \frac{\Gamma[-s_{0l}]}{\Gamma \left[\frac{1 - s_{0l} - E/\hbar\omega}{2} \right]} \left(\frac{R}{a_\mu} \right)^{s_{0l}} \\ & + \frac{\Gamma[s_{0l}]}{\Gamma \left[\frac{1 + s_{0l} - E/\hbar\omega}{2} \right]} \left(\frac{R}{a_\mu} \right)^{-s_{0l}}. \end{aligned} \quad (38)$$

From this we can derive a transcendental equation that determines the energy spectrum as a function of R_t [25]

$$-|s_{0l}| \ln \left(\frac{R_t}{a_\mu} \right) = \arg \left\{ \frac{\Gamma \left[\frac{1 + s_{0l} - E}{2} \right]}{\Gamma[1 + s_{0l}]} \right\} \mod \pi. \quad (39)$$

The energy spectrum is unbounded from above and below. We index the states with $q \in \mathbb{Z}$, and define the $q = 0$ state to be the first positive energy state at $R_t/a_\mu = \exp(\pi/|s_{0l}|)$ with $q > 0$ referring to higher energy states and $q < 0$ to lower energy states. For example for $R_t/a_\mu = 1$ and $s_{0l} = i \cdot 1.006$, the energies corresponding to $q = 3, 2, 1, 0, -1, -2$ are given $E_{\text{rel}}/\hbar\omega \approx 6.60, 4.48, 2.27, -0.85, -566, -291649$ respectively and at $R_t/a_\mu = \exp(\pi/|s_{0l}|)$ the energies corresponding to $q = 3, 2, 1, 0, -1, -2$ are given $E_{\text{rel}}/\hbar\omega \approx 8.686, 6.60, 4.48, 2.27, -0.85, -566$. In general the energy of the $q = N$ state at $R_t/a_\mu = \exp(\pi/|s_{0l}|)$ is equal to the energy at $R_t/a_\mu = 1$ of the $q = N + 1$ state. For fixed R_t the states with $q \geq 0$ have a regular spacing of $\approx 2\hbar\omega$ whereas the spacing of the $q < 0$ states is grows larger for more negative energies.

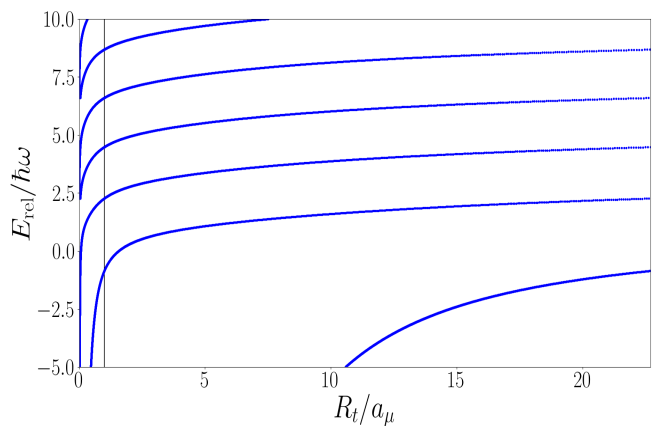


FIG. 5. The energy spectrum for Efimov states as defined by Eq. (39). Calculated using $s = i \cdot 1.006$. The upper limit on the horizontal axis is $e^{\pi/|s|} \approx 22.7$, and the vertical black line is $R_t = a_\mu$.

Physically speaking the additional parameter R_t is needed because in the Efimov states the specifics of the interparticle interaction become significant, due to the attractive s_{0l}^2/R^2 potential term, and can no longer accurately be considered a contact interaction. R_t describes the short-range (but not zero-range) properties of the interparticle interaction and will, in general, differ for different species of atoms although some work suggests that it will vary little in practice [32].

Efimov states also exist in the fermionic case for sufficient mass imbalance [27, 29]. By solving Eq. (32) for κ , with $s_{nl} = 0$ and $\eta = -1$, we find the mass imbalance for which s_{nl} becomes imaginary and Efimov states are then allowed. There are no Efimov states for l is even. They appear for $l = 1, 3, 5, \dots$ for $\kappa \gtrsim 13.606, \dots, 75.994, \dots, 187.958, \dots$ respectively. This is in good agreement with previous work [29–31]. Using the method of Section II A, the Efimov states appear (or do not appear as appropriate) at these predicted values of l and κ .

As described above; in the method of Section II A the

Efimov energies depend on matrix size and are divergent with increasing matrix size, and in the approach of Section II B the Efimov energies are not fixed so an additional parameter is required. In fact these two methods, the matrix size and the three-body parameter, are closely linked; for every finite matrix size there is a value of R_t that produces the same Efimov energy spectrum to a high degree of accuracy. This result implies that the boundary condition Eq. (37) is enforced by the finite matrix size of Eq. (17). The errors between the Efimov energies calculated with the two methods is given in Tables II and III.

In Tables II and III the value of R_t is calculated by substituting the lowest Efimov energy calculated with the matrix method for a given N into Eq. (39). The lowest Efimov energy state corresponds to either $q = 0$ or $q = -1$ depending on N and the particle symmetry. The $q < -1$ states have such extreme and far apart energies that there are significant numerical challenges in evaluating with the method of Section II A. As such we are unable to confirm if the method of Section II A predicts these Efimov states, however it is unlikely that they are predicted. In Figs. 1, 2, and 3 the unitary states smoothly transition to non-interacting states as $a_s \rightarrow 0$ and additional lower energy states would non-physically change the multiplicity of the non-interacting ground state.

The error is $\lesssim 1\%$ for all calculated values and is most likely due to the linear interpolation required to determine the unitary energies using the method of Section II A.

III. CONCLUSION

In this work we have considered exact solutions for three particles in a spherically symmetric trap. We have provided results for both fermionic systems with mass imbalance and bosonic systems where by definition there is no mass imbalance. In each case these results can be used to investigate physical phenomena such as quench dynamics [6, 9–18] and the derivation of the equation of state of such a gas [19–23].

We have also revisited, for fermions with mass imbalance, and bosons, the Efimov states in such systems. Specifically we have compared solutions with the matrix approach, Section II A, and the hyperspherical approach, Section II B. We find in each case very good agreement between the two approaches, at unitarity, for fermions with and without mass imbalance and for mass-balanced bosons. Finally, we have investigated, in Section II C the emergence of Efimov states for the mass-imbalanced fermion case and the mass-balanced boson case. Remarkably we find a connection between the matrix and effec-

tive range approaches in determining the energy of Efimov states. Specifically, for the matrix approach we find the energy of an Efimov state diverges with increasing matrix size, see Fig. 4. However for every matrix size

Bosons	$q = 0$	$q = 1$	$q = 2$	$q = 3$	$q = 4$
$N = 10$	-0.563	2.393	4.612	6.747	8.849
$R_t/a_\mu = 1.131$	-0.563	2.365	4.566	6.682	8.763
Error %	0	1.191	1.000	0.963	0.967
	$q = -1$	$q = 0$	$q = 1$	$q = 2$	$q = 3$
$N = 20$	-1.531	2.112	4.353	6.490	8.588
$R_t/a_\mu = 18.216$	-1.531	2.094	4.326	6.455	8.544
Error %	0	0.870	0.621	0.543	0.511
$N = 30$	-2.428	1.943	4.198	6.341	8.441
$R_t/a_\mu = 14.897$	-2.428	1.928	4.178	6.315	8.409
Error %	0	0.767	0.494	0.410	0.375
$N = 40$	-3.301	1.823	4.087	6.234	8.336
$R_t/a_\mu = 12.912$	-3.301	1.810	4.070	6.212	8.310
Error %	0	0.709	0.423	0.344	0.310
$N = 50$	-4.164	1.731	4.001	6.150	8.253
$R_t/a_\mu = 11.555$	-4.164	1.719	3.990	6.131	8.231
Error %	0	0.681	0.386	0.303	0.266

TABLE II. Comparison of the matrix and three-body parameter energies (in units of $\hbar\omega$) for bosons. The three-body parameter is found by substituting the lowest unitary Efimov energy predicted by the matrix method into Eq. (39). For $N = 10$ this means that the $q = 0$ state is the corresponding lowest energy state, and for $N \geq 20$ $q = -1$ is the corresponding state. All values are stated to 3 decimal places. Errors are $\lesssim 1\%$, with the primary source of error being the accurate calculation of the matrix energies, this also affects the accuracy of R_t as R_t is chosen depending on the lowest Efimov state energy.

there is a value of R_t that produces the same energy spectrum, see Tables II and III.

IV. DATA AVAILABILITY STATEMENT

All data will be provided upon request to A. D. Kerin.

V. ACKNOWLEDGEMENTS

A.D.K. is supported by an Australian Government Research Training Program Scholarship and by the University of Melbourne.

With thanks to Victor Colussi for enlightening conversations.

[1] T. Busch, B.-G. Englert, K. Rzażewski, and M. Wilkens, Foundations of Physics **28**, 549 (1998).

[2] D. V. Fedorov and A. Jensen, Journal of Physics A:

Fermions	$q = 0$	$q = 1$	$q = 2$	$q = 3$	$q = 4$
$N = 10$	1.507	3.626	5.713	7.787	9.857
$R_t/a_\mu = 2.59 \times 10^7$	1.507	3.611	5.680	7.731	9.773
Error %	0	0.380	0.573	0.721	0.8544
$N = 20$	1.433	3.525	5.588	7.640	9.685
$R_t/a_\mu = 1.84 \times 10^7$	1.43	3.51	5.57	7.61	9.65
Error %	0	0.150	0.221	0.272	0.312
$N = 30$	1.397	3.477	5.531	7.574	9.611
$R_t/a_\mu = 1.50 \times 10^7$	1.397	3.474	5.524	7.563	9.594
Error %	0	0.085	0.127	0.153	0.178
$N = 40$	1.374	3.447	5.496	7.535	9.567
$R_t/a_\mu = 1.30 \times 10^7$	1.374	3.445	5.491	7.526	9.556
Error %	0	0.061	0.087	0.106	0.121
$N = 50$	1.355	3.425	5.463	7.491	9.515
$R_t/a_\mu = 1.14 \times 10^7$	1.355	3.421	5.463	7.496	9.523
Error %	0	0.113	0.005	0.063	0.082

TABLE III. Comparison of the matrix and three-body parameter energies (in units of $\hbar\omega$) for fermions with $\kappa = 13.75$ and $l = 1$. The three-body parameter is found by substituting the lowest unitary Efimov energy predicted by the matrix method into Eq. (39). All values are stated to 3 decimal places. Errors are $\lesssim 1\%$, with the primary source of error being the accurate calculation of the matrix energies, this also affects the accuracy of R_t as R_t is chosen depending on the lowest Efimov state energy.

- Mathematical and General **34**, 6003 (2001).
- [3] F. Werner and Y. Castin, Physical Review Letters **97**, 150401 (2006).
- [4] J. Kestner and L.-M. Duan, Physical Review A **76**, 033611 (2007).
- [5] K. M. Daily and D. Blume, Physical Review A **81**, 053615 (2010).
- [6] B. C. Mulkerin, C. J. Bradly, H. M. Quiney, and A. M. Martin, Physical Review A **86**, 053631 (2012).
- [7] F. Werner and Y. Castin, Physical Review A **74**, 053604 (2006).
- [8] D. Blume, Reports on Progress in Physics **75**, 046401 (2012).
- [9] X.-J. Liu, H. Hu, and P. D. Drummond, Physical Review Letters **102**, 160401 (2009).
- [10] X.-J. Liu, H. Hu, and P. D. Drummond, Physical Review A **82**, 023619 (2010).
- [11] X. Cui, Few Body Systems **52**, 65 (2012).
- [12] T. Stöferle, H. Moritz, K. Günter, M. Köhl, and T. Esslinger, Physical Review Letters **96**, 030401 (2006).
- [13] D. Rakshit, K. M. Daily, and D. Blume, Physical Review A **85**, 033634 (2012).
- [14] D. B. Kaplan and S. Sun, Physical Review Letters **107**, 030601 (2011).
- [15] B. Mulkerin, C. Bradly, H. Quiney, and A. Martin, Physical Review A **85**, 053636 (2012).
- [16] S. Nascimbène, N. Navon, K. Jiang, F. Chevy, and C. Salomon, Nature **463**, 1057 (2010).
- [17] M. Ku, A. Sommer, L. Cheuk, and M. Zwierlein, Science **335**, 563 (2012).
- [18] J. Levinsen, P. Massignan, S. Endo, and M. M. Parish, Journal of Physics B: Atomic, Molecular and Optical Physics **50**, 072001 (2017).
- [19] G. Bougas, S. Mistakidis, G. Alshalan, and P. Schmelcher, Physical Review A **102**, 013314 (2020).
- [20] G. Bougas, S. I. Mistakidis, and P. Schmelcher, Physical Review A **100**, 053602 (2019).
- [21] L. Budewig, S. Mistakidis, and P. Schmelcher, Molecular Physics **117**, 2043 (2019).
- [22] L. M. A. Kehrberger, V. J. Bolsinger, and P. Schmelcher, Physical Review A **97**, 013606 (2018).
- [23] A. Kerin and A. Martin, Physical Review A **102**, 023311 (2020).
- [24] J. P. D’Incao, J. Wang, and V. E. Colussi, Physical Review Letters **121**, 023401 (2018).
- [25] S. Jonsell, H. Heiselberg, and C. Pethick, Physical Review Letters **89**, 250401 (2002).
- [26] D. Blume and K. Daily, Physical review letters **105**, 170403 (2010).
- [27] V. Efimov, Nuclear Physics A **210**, 157 (1973).
- [28] V. N. Efimov, *WEAKLY BOUND STATES OF THREE RESONANTLY INTERACTING PARTICLES.*, Tech. Rep. (Ioffe Inst. of Physics and Tech., Leningrad, 1970).
- [29] O. Kartavtsev and A. Malykh, Journal of Physics B: Atomic, Molecular and Optical Physics **40**, 1429 (2007).
- [30] O. Kartavtsev and A. Malykh, JETP letters **86**, 625 (2008).
- [31] S. Endo, P. Naidon, and M. Ueda, Few-Body Systems **51**, 207 (2011).
- [32] J. Wang, J. D’Incao, B. Esry, and C. H. Greene, Physical review letters **108**, 263001 (2012).
- [33] H. Bethe and R. Peierls, Proceedings of the Royal Society of London. Series A-Mathematical and Physical Sciences **148**, 146 (1935).
- [34] E. Braaten and H.-W. Hammer, Physics Reports **428**, 259 (2006).
- [35] F. Werner, Theses, Université Pierre et Marie Curieâ Paris VI, Paris France (2008).
- [36] T. Kraemer, M. Mark, P. Waldburger, J. G. Danzl, C. Chin, B. Engeser, A. D. Lange, K. Pilch, A. Jaakkola, H.-C. Nägerl, *et al.*, Nature **440**, 315 (2006).